

# Transient growth on boundary layer streaks

By JÉRÔME HËPFFNER, LUCA BRANDT,  
AND DAN S. HENNINGSON

KTH Mechanics, S-100 44 Stockholm, Sweden

(Received 4 May 2005)

The linear perturbations evolving on streamwise boundary layer streaks which yield maximum energy growth are computed. The steady and spanwise periodic streaks arising from the nonlinear saturation of optimally growing streamwise vortices are considered as base flow. It is shown that significant transient growth may occur for both sinuous antisymmetric perturbations and for varicose symmetric modes. The energy growth is observed at amplitudes significantly below the threshold beyond which the streaks become linearly unstable and is largest for sinuous perturbations, to which the base flow considered first become unstable. The optimal initial condition consists of velocity perturbations localised in the regions of highest shear of the streak base flow, tilted upstream from the wall. The optimal response is still localised in the areas of largest shear but it is tilted in the flow direction. The most amplified perturbations closely resemble the unstable eigenfunctions obtained for streaks of higher amplitudes. The results suggest the possibility of a transition scenario characterised by the non-modal growth of primary perturbations, the streaks, followed by the secondary transient growth of higher frequency perturbations. Implication for turbulent flow is also discussed.

---

## 1. Introduction

Eigenvalue analysis is traditionally performed to investigate the linear stability of a given flow configuration. The least stable among the exponentially decaying eigensolutions to the linearised disturbance equations provides information about the flow behaviour at large times. However, initial conditions which give transient energy growth may exist, a possibility related to the non-normality of the governing operator. This transient energy amplification is also referred to as non-modal since it is not due to the behaviour of a single eigenmode but it is caused by the superposition of several of them. In some cases the energy growth can be large enough to trigger nonlinear interactions and take the flow into a new configuration. The initial disturbance able to induce the largest perturbation at a given time is called *optimal* and can be computed applying optimisation techniques. These were first introduced in this context by Farrell (1988).

Here we apply this analysis to investigate the behaviour of small amplitude perturbations developing on boundary layer streamwise streaks. These elongated structures and their breakdown are found to be key factors both in transition in boundary layers subject to high levels of free-stream turbulence (Matsubara & Alfredsson 2001) and in the near wall region in turbulent flows (e.g. Kim, Kline & Reynolds 1971). The motivation for this study comes from the observation that the breakdown may occur also for asymptotically stable streaks. In the case of near-wall turbulence, it was noted by Schoppa & Hussain (2002) that only 20% of the streaks in the buffer layer exceed the amplitude threshold for instability. By choosing an initial condition based on streamwise- spanwise-velocity

Reynolds stress events from fully developed near-wall turbulence, these authors were able to identify a *streak transient growth* mechanism, capable of triggering the breakdown. The amplification observed was about tenfold. From the experimental data on transition induced by free-stream turbulence as well as from the recent simulations by Brandt, Schlatter & Henningson (2004) it is difficult to assess whether the streaks undergoing breakdown are linearly unstable. However, the possibility of a transient energy amplification is suggested by the experiments of Lundell (2004). In the present study, by considering a steady approximation of the transitional streaks, we assess how large this transient growth can be and present the corresponding optimal flow structures. The present results are therefore directly applicable to boundary layer transition, albeit with physical connection with near-wall turbulence via rescaling of the base flows.

Interestingly, the basic flow under consideration is also the result of a non-modal growth. Owing to the lift-up effect (Landahl 1975), streamwise elongated vortices are able to mix high- and low-momentum fluid and thus create streaks of high and low streamwise velocity. It is therefore not surprising that for wall-bounded laminar flows the initial condition yielding the largest transient energy growth has been found to consist of streamwise oriented vortices of long streamwise wavelength (see Schmid & Henningson 2001, for a review). In the case of a spatially evolving zero-pressure-gradient boundary layer, the input at the leading edge leading to maximum output energy far downstream has been identified by Andersson, Berggren & Henningson (1999) and Luchini (2000). The output perturbation consists of streamwise streaks whose spanwise periodicity is of the order of the boundary layer thickness. If the upstream vortex amplitude is high enough, the disturbance eventually reach an amplitude at which nonlinear effects become relevant. The basic flow considered here was obtained in Andersson *et al.* (2001) by computing the nonlinear streaks forced by these optimal leading edge vortices.

If the amplitude of the streaks grow to a sufficiently high value, instabilities can develop and provoke breakdown to turbulence. This instability is caused by inflectional profiles of the base flow velocity and it is of inviscid type. The experiments of Swearingen & Blackwelder (1987) were the first to document the emergence of streaks with inflectional profiles, in this case owing to the formation of Görtler vortices in the boundary layer over a concave wall. This investigation demonstrated that time-dependent fluctuations appear in the flow either in a spanwise symmetric (varicose) or antisymmetric (sinuous) pattern with respect to the underlying streak. The varicose perturbations are more closely related with the wall-normal inflection points while the sinuous oscillations are related with the spanwise inflectional profile and they were found to be the fastest growing. For the streaks considered here, it was also found that the most dangerous perturbations are of sinuous type (Brandt & Henningson 2002) and that the instability is convective in nature (Brandt *et al.* 2003).

The inviscid streak instability evolves on the fast convective time scale and is characterised by a large exponential growth. Therefore, we will focus our analysis on streaks of moderate amplitude, mainly stable to linear perturbations, to investigate the potentiality of a non-modal growth mechanism to trigger the breakdown of subcritical streaks.

## 2. Flow configuration and numerical method

### 2.1. Base flow and physical configuration

We consider the boundary layer over a flat plate and define the local Reynolds number,  $Re = (U_\infty \delta_*)/\nu$ , by means of the free-stream velocity  $U_\infty$  and the local Blasius boundary layer displacement thickness  $\delta_*$ . In the analysis the streaks resulting from the nonlinear

evolution of the spatial optimal perturbation in a zero pressure gradient boundary layer are considered. This base flow was computed in Andersson *et al.* (2001) by solving the full Navier–Stokes equations. In that work, the complete velocity field representing the steady linear optimal perturbation calculated by Andersson *et al.* (1999) was used as input close to the leading edge and its downstream nonlinear development was monitored for different upstream amplitudes of the input disturbance. The flow was assumed periodic in the spanwise direction and only one spanwise wavelength of the optimal perturbation considered. To quantify the size of this primary disturbance field at each streamwise position, an amplitude  $A$  was defined in Andersson *et al.* (2001) as

$$A(X) = \frac{1}{2} \left[ \max_{y,z} \left( U(x, y, z) - U_B(x, y) \right) - \min_{y,z} \left( U(x, y, z) - U_B(x, y) \right) \right], \quad (2.1)$$

where  $U_B(x, y)$  is the Blasius profile and  $U(x, y, z)$  is the total streamwise velocity in the presence of streaks. The streamwise velocity  $U$  is made non dimensional with respect to the free-stream velocity  $U_\infty$ . The spanwise wavenumber is taken to be  $\beta = 0.45$ , which corresponds to linearly optimally growing streaks at  $x = 1$  (cf. the scaling adopted in Andersson *et al.* 2001).

We are interested in determining the local properties of the streaks in the parallel flow approximation. Therefore one wishes to study the local characteristics of a basic flow which evolves slowly in the streamwise direction, as required in the boundary layer approximation and to consider a perturbation which evolves faster than the basic flow. The parallel flow assumption becomes therefore questionable for perturbations of long streamwise scale or when the behavior at large times is considered.

As in Andersson *et al.* (2001), the streak profiles under consideration are extracted at the streamwise station  $x = 2$ . This station has been chosen because it is associated with the region where the streak energy attains its maximum value (see figure 5 in Andersson *et al.* 2001). The critical amplitude  $A$  beyond which unstable streamwise travelling waves are found is 0.26 for sinuous instability modes and 0.37 for their varicose counterpart. Note finally that in the present investigation, we restrict our attention to perturbations which have the same spanwise periodicity as the base flow, i.e. according to Floquet theory the detuning parameter is taken to be zero (see Nayfeh & Mook 1979). This reduction to the fundamental mode amounts to considering a total flow (basic flow plus perturbation) which is spanwise periodic of fundamental wavelength  $\lambda_z$  and it is justified by the observation that the perturbations under consideration are localised in the region of strongest shear. For this reason, weak variations with the Floquet parameter were found in the eigenvalue analysis in Andersson *et al.* (2001).

## 2.2. Governing equations and optimisation procedure

The equations governing the linear evolution of a perturbation velocity  $\mathbf{u}(x, y, z, t) = (u, v, w)$ , of corresponding pressure  $p$ , on the streak profile  $U(y, z)$  are obtained by substituting  $U + \mathbf{u}$  into the Navier–Stokes equations and neglecting the quadratic terms in the perturbation. Following a procedure similar to that used in the derivation of the Orr–Sommerfeld and Squire system, the above equations can be reduced to two equations in terms of the normal velocity  $v$  and the normal vorticity  $\eta = u_z - w_x$  (Waleffe 1995; Schmid & Henningson 2001)

$$\begin{cases} \Delta v_t + U \Delta v_x + U_{zz} v_x + 2U_z v_{xz} - U_{yy} v_x - 2U_z w_{xy} - 2U_{yz} w_x = \frac{1}{Re} \Delta \Delta v, \\ \eta_t + U \eta_x - U_z v_y + U_{yz} v + U_y v_z + U_{zz} w = \frac{1}{Re} \Delta \eta. \end{cases} \quad (2.2)$$

In the above, the spanwise velocity  $w$  can be eliminated by using the identity

$$w_{xx} + w_{zz} = -\eta_x - v_{yz}.$$

Since the flow is assumed parallel, solution can be sought in the form of normal modes

$$[v, \eta] = [\hat{v}(y, z, t), \hat{\eta}(y, z, t)] e^{i\alpha x} + c.c. \quad (2.3)$$

where  $\alpha$  is the streamwise wavenumber. As the basic flow is symmetric about  $z = 0$ , the modes can be further divided into separate classes according to their odd or even symmetry with respect to the basic flow.

In particular, fundamental modes with an odd symmetry are called varicose with reference to their streamline patterns in the  $(x, z)$  plane, whereas fundamental modes with an even symmetry are usually referred to as sinuous.

Being able to describe the dynamics of small perturbations on streamwise streaks, we aim at finding the initial disturbance that would lead to the largest amplification at a given time. The search for the initial condition that leads to the maximum energy growth for a linear system is a well-known procedure, (see e.g. Andersson *et al.* 1999; Corbett & Bottaro 2000) and it is therefore only briefly outlined here.

Let us define  $\mathcal{H}_\tau$  as the linear operator that maps an arbitrary initial condition  $q$  to the subsequent state at time  $\tau$ . To apply this operator amounts to integrating (2.2) in time. The maximum energy growth  $G(\tau)$  at time  $\tau$  is

$$G(\tau) = \max_q \frac{\|\mathcal{H}_\tau q\|}{\|q\|} = \max_q \frac{(\mathcal{H}_\tau q, \mathcal{H}_\tau q)}{(q, q)} \triangleq \max_q \frac{(q, \mathcal{H}_\tau^+ \mathcal{H}_\tau q)}{(q, q)}, \quad (2.4)$$

where the rightmost identity introduces the definition of  $\mathcal{H}_\tau^+$ , the adjoint of  $\mathcal{H}_\tau$  with respect to the inner product  $(\cdot, \cdot)$ . It appears from (2.4) that the greatest eigenvalue and corresponding eigenvector of the operator  $\mathcal{H}_\tau^+ \mathcal{H}_\tau$  are the greatest achievable growth and the corresponding initial condition.

The direct solution of the problem by eigendecomposition of  $\mathcal{H}_\tau^+ \mathcal{H}_\tau$  is a heavy computational task for a system of large order, since it involves the computation of two matrix exponentials for the explicit description of  $\mathcal{H}_\tau$  and  $\mathcal{H}_\tau^+$ . Instead, the mapping  $\mathcal{H}_\tau$  is applied to the state  $q(0)$  by marching the initial condition in time using the dynamic operator  $L$ , defined by (2.2), and  $\mathcal{H}_\tau^+$  is applied to  $q(\tau)$  by marching the state backward in time using the adjoint  $L^+$  of the dynamic operator. The adjoint  $L^+$  is built as the discrete adjoint

$$L^+ = Q^{-1} L^H Q, \quad (2.5)$$

where the matrix  $Q$  defines the discrete energy inner product,

$$(q_1, q_2) = q_2^H Q q_1, \quad (2.6)$$

and the superscript  $H$  stands for the matrix conjugate transpose. Each step of the power iteration  $q^{n+1} = \mathcal{H}_\tau^+ \mathcal{H}_\tau q^n$  will magnify the projection of  $q$  onto the desired flow state by a factor  $G$ . The iteration will thus converge quickly provided the leading eigenvalue is well separated from the following ones. In the present case, an absolute accuracy of  $10^{-2}$  could be achieved within about 15 iterations when starting from an arbitrary initial guess.

The state variable and dynamic operator are discretized in the wall-normal direction using a Chebyshev collocation method (see e.g. Weideman & Reddy 2000). Both the forward and the backward time marching are implemented using the second-order Crank-Nicholson scheme (implicit) and a unit time step is employed in the time integration.

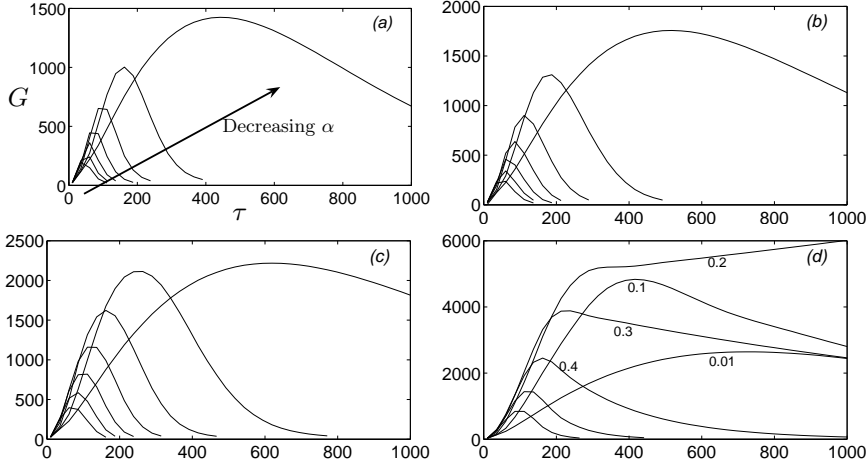


FIGURE 1. Maximum amplification  $G$  versus  $\tau$  of sinuous perturbations with wavenumber  $\alpha = 0.01, 0.1, 0.2 \dots 0.6$  for streak of increasing amplitude. (a):  $A = 0.14$ , (b):  $A = 0.20$ , (c):  $A = 0.255$ , (d):  $A = 0.288$ . Note the appearance of the exponential instability for the largest streak amplitude.

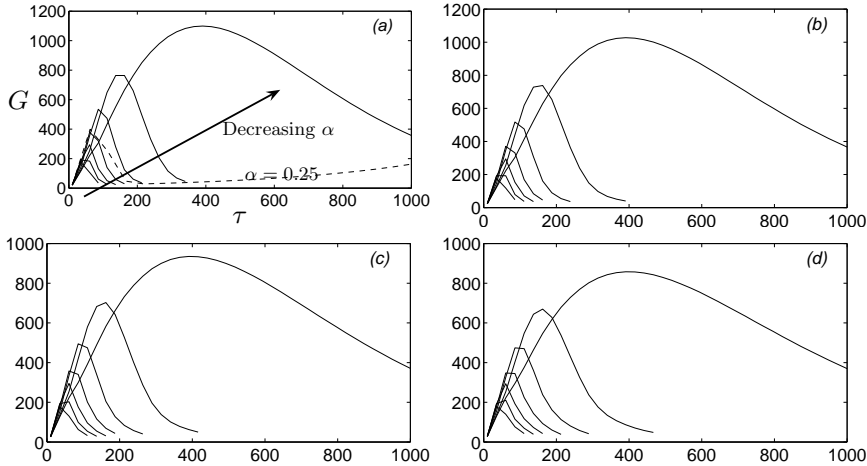


FIGURE 2. Maximum amplification  $G$  versus  $\tau$  of varicose perturbations with wavenumber  $\alpha = 0.01, 0.1, 0.2 \dots 0.6$  for streak of increasing amplitude. (a):  $A = 0.14$ , (b):  $A = 0.20$ , (c):  $A = 0.255$ , (d):  $A = 0.288$ . The dashed line in (a) pertains to  $\alpha = 0.25$  at which a viscous instability is present.

The results have been validated by computing the evolution of the optimal input with the numerical code and procedure described in Brandt *et al.* (2003).

### 3. Results

#### 3.1. Optimal growth

The maximum energy growth  $G(\tau)$  for different values of the streak amplitude and of the streamwise wavenumber  $\alpha$  is displayed in figure 1 and 2 for the sinuous and varicose symmetry respectively. The curve given by  $G(\tau)$  represents the maximum possible amplification at each instant in time optimised over all possible initial conditions with unity energy norm. Since the optimal initial conditions are in general different for different

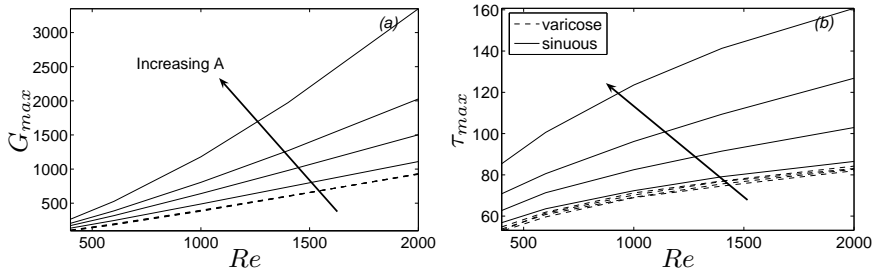


FIGURE 3. (a) Maximum transient growth versus Reynolds number and (b) instant of maximum amplification versus the Reynolds number for streaks of increasing amplitude,  $A = 0.14, 0.20, 0.229, 0.255, 0.288$ . Solid lines display sinuous perturbations whereas dashed lines are used for their varicose counterpart. The selected streamwise wavenumber is  $\alpha = 0.3$ .

$\tau$ ,  $G(\tau)$  can be also thought of as the envelope of the energy evolutions of the initial conditions yielding maximum energy growth at each instant  $\tau$ . Note that time is made non-dimensional with respect to  $\delta^*/U_\infty$ .

Results are presented also for low values of the streamwise wavenumber  $\alpha$ , at which the parallel flow approximation becomes questionable, to show that the maximum amplification is attained in the limit of  $\alpha \rightarrow 0$  for asymptotically stable streaks. However, significant amplification is observed also at larger wave numbers. For sinuous perturbations, an energy growth of the order of a thousand is found at  $Re = 1000$  already for a streak amplitude of 14%, i.e. well below the threshold for the onset of the inviscid secondary instability. It can also be seen in figure 1 that the energy growth of perturbations of larger  $\alpha$  increases with increasing streak amplitude more than for disturbance of low streamwise wavenumber. Figure 1(d) shows the maximum energy growth for a streak which is slightly unstable to sinuous perturbations,  $A = 0.288$ . The initial transient growth becomes stronger, it is no longer maximum at the lowest streamwise wavenumber considered and for the unstable  $\alpha = 0.2$ , it dominates over the exponential growth for times  $\tau < 200$ . Conversely, for streaks of higher amplitudes ( $> 30\%$ ), the exponential inviscid instability is seen to become dominant already at small values of  $\tau$  (not reported here).

The results pertaining to varicose perturbations are presented in figure 2. The maximum transient energy amplification is lower than for sinuous perturbations and it is slightly decreasing with increasing streak amplitude. The dashed line in figure 2(a) depicts perturbations with  $\alpha = 0.25$  at which a weak viscous instability is present (see Cossu & Brandt 2004).

The maximum transient growth and the instant at which the maximum occurs are displayed in figure 3 versus the Reynolds number for sinuous and varicose perturbations with  $\alpha = 0.3$ . Both these quantities increase with  $Re$  but a simple scaling law could not be found. Note that in the simulations by Brandt *et al.* (2004) of a boundary layer subject to free-stream turbulence of relatively high intensity,  $Tu = 4.7\%$ , transition is found to occur, in average, at  $Re \approx 730$ , whereas in the experiment by Matsubara & Alfredsson (2001), where  $Tu \approx 2\%$ , the breakdown to turbulence is observed at  $Re \approx 1500$ .

### 3.2. Flow visualisation

The velocity field pertaining to the initial conditions yielding maximum growth and the flow configuration at the time of maximum energy are displayed in figure 4 and 5 for sinuous and varicose disturbances, respectively. In the case of antisymmetric perturbations, the streamwise and wall-normal velocity components of the optimal disturbance

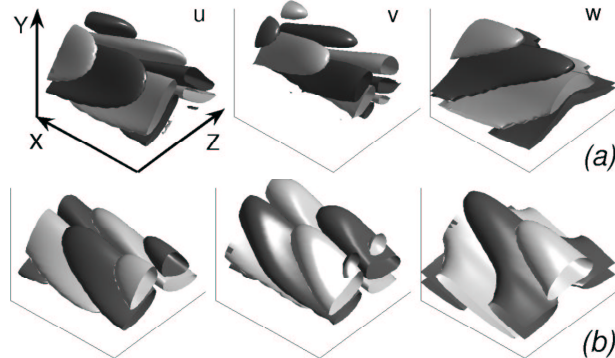


FIGURE 4. (a) Streamwise, wall-normal and spanwise velocity fields of the input initial condition yielding maximum output energy at  $\tau = 123$  for sinuous perturbations with  $\alpha = 0.3$  at  $Re = 1000$ . (b) Velocity field at the instant of maximum growth. The isosurfaces represent the areas where the value of the velocity is 0.2 of the maxima, which are  $u = 0.386$ ,  $v = 0.658$  and  $w = 1.893$  at  $t = 0$ ;  $u = 63.499$ ,  $v = 6.13$  and  $w = 15.662$  at  $t = \tau$ .

are concentrated in the region of strongest spanwise shear of the basic flow, i.e. on the flanks of the low-speed streak located in the middle of the box in the figures presented here, whereas the spanwise velocity is larger in the region of strong wall-normal shear on the top of the high-speed streak. Both three velocity components are tilted upstream from the wall. The optimal response velocity field (fig. 4b) resembles the unstable modes leading to the streak breakdown (see Brandt & Henningson 2002). As a consequence, it would be difficult to assess from experimental results whether the streak breakdown is triggered by an exponential instability or by a non-modal mechanism. The streamwise velocity component is the most amplified and the perturbation is still located in the region of strongest shear but the flow structures are now inclined in the downstream direction. This indicates that the disturbance has extracted energy from the mean shear by transporting momentum down the mean velocity gradient, similarly to what is observed for the Orr mechanism (Orr 1907; Butler & Farrell 1992). This non-modal growth mechanism is the only present in the case of spanwise independent perturbations in a shear flow and describes short term inviscid instabilities due to the tilting of initial disturbances into the direction of the mean shear. However, the maximum of the perturbation is not attained when the disturbance is aligned in the wall-normal direction (cf. Butler & Farrell 1992) and indeed the analysis presented below confirms that other mechanisms are active as well.

In the case of varicose perturbations (figure 5), the rotation of the perturbation from upstream to downstream tilting is also observed. The perturbations are still located at the locations of maximum shear of the underlying streak and the streamwise velocity component is the most amplified.

To try to better understand the mechanisms responsible for the observed growth, the evolution of the perturbation kinetic energy  $K$  integrated over one streamwise wavelength is considered

$$K_t = \int \left( \underbrace{-uv U_y}_{T_y} \underbrace{-uw U_z}_{T_z} \underbrace{-\boldsymbol{\omega} \cdot \boldsymbol{\omega} / Re}_D \right) dy dz dx, \quad (3.1)$$

where  $\boldsymbol{\omega}$  is the perturbation vorticity vector. This balance equation is derived in a straightforward manner from the Navier-Stokes equations linearised around the base flow  $U(y, z)$ . The first production term of density  $T_y = -uv U_y$  represents the work of

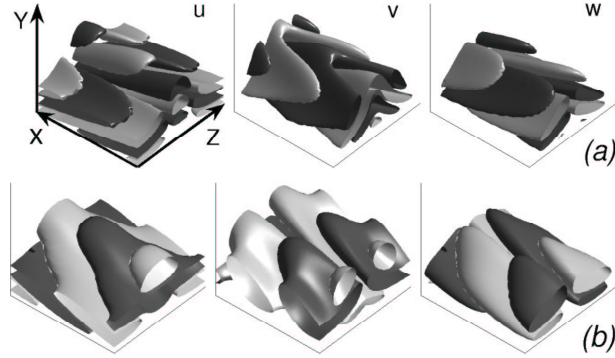


FIGURE 5. (a) Streamwise, wall-normal and spanwise velocity fields of the input initial condition yielding maximum output energy at  $\tau = 80$  for varicose perturbations with  $\alpha = 0.3$  at  $Re = 1000$ . (b) Velocity field at the instant of maximum growth. The isosurfaces represent the areas where the value of the velocity is 0.2 of the maxima, which are  $u = 0.462$ ,  $v = 0.867$  and  $w = 1.494$  at  $t = 0$ ;  $u = 27.691$ ,  $v = 3.538$  and  $w = 8.560$  at  $t = \tau$ .

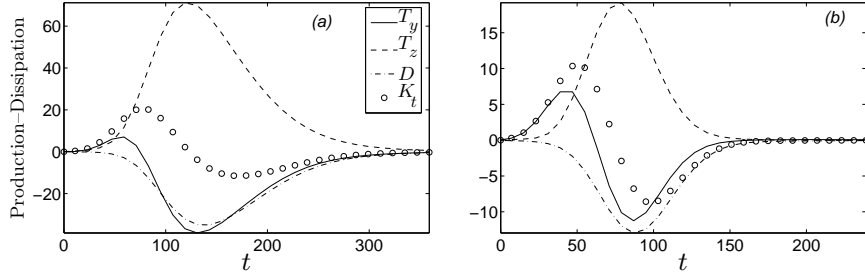


FIGURE 6. Time evolution of the volume integral of the terms appearing in the perturbation kinetic energy equation. —:  $T_y = -uvU_y$ , ---:  $T_z = -uwU_z$ , ·-·-: viscous dissipation and  $\circ$ :  $K_t$ . (a) Sinuous perturbation at  $Re = 1000$ ,  $\alpha = 0.3$ ,  $\tau = 123$ . (b) Varicose perturbation at  $Re = 1000$ ,  $\alpha = 0.3$ ,  $\tau = 80$ .

the Reynolds stress  $-uv$  on the wall-normal basic shear  $U_y$ , while the second production term of density  $T_z = -uwU_z$  is associated with the work of the Reynolds stress  $-uw$  on the spanwise basic shear  $U_z$ . The last term represents viscous dissipation.

The time evolution of the terms appearing in equation (3.1) is displayed in figure 6 both for a sinuous and a varicose perturbation. The production associated to the wall-normal shear of the perturbation  $T_y$  is positive at early times and then becomes negative as for two-dimensional perturbations experiencing a growth due to the Orr mechanism. However its amplitude is lower than that of the production related to the spanwise shear  $T_z$  which is therefore responsible for the large growth observed both for the sinuous and the varicose disturbance. It is remarkable to note that initially both production terms are positive and that the spanwise shear is also responsible for the growth of varicose perturbations. This is unexpected considering that exponentially growing varicose perturbations are driven by the action of the wall-normal shear. Two growth mechanisms seem therefore to be active, similarly to what observed in constant-shear flows by Farrell & Ioannou (1993). Tilting of the mean flow vorticity, as in the streak generation process in two-dimensional flows, and the Orr mechanism. The former is stronger for  $\alpha \rightarrow 0$ , while the latter is present at finite  $\alpha$ .



#### 4. Conclusions

The behaviour of linear perturbations developing on boundary layer streamwise streaks is investigated for streak amplitudes below or right at the onset of the inflectional secondary instability. The input velocity fields leading to an output flow of maximum possible energy at a given time are computed for the first time for a parallel basic flow periodic in the spanwise direction.

It is found that large energy amplification can be achieved both by sinuous and by varicose disturbances. The transient energy growth is larger for sinuous modes, it increases with the Reynolds number and it is already relevant at amplitudes well below the threshold for the onset of secondary instabilities. The results indicate the possibility, first suggested by Grossmann (2000), of a transition scenario in which energy is extracted from the laminar state by a series of linear non-modal mechanisms. In particular, first the lift-up effect responsible for the streak growth and then the non-modal amplification of the streamwise dependent perturbations presented here.

The present results have also implications on the dynamics of near-wall turbulent flows, where the streak breakdown is one of the key elements of the underlying self-sustaining process. The regeneration of vortices following the streak breakdown can be related to non-modal growth mechanisms and therefore occur at lower streak amplitudes (cf. Schoppa & Hussain 2002) and for both sinuous and varicose perturbations.

The input and output velocity fields are also presented. The optimal initial condition consists of velocity perturbations localised in the regions of highest shear of the streak base flow, tilted upstream from the wall. The optimal response is still localised in the areas of largest shear but it is tilted in the flow direction. The most amplified perturbations closely resemble the unstable eigenfunctions obtained for streaks of higher amplitudes and it appears therefore difficult to distinguish between the two from experimental/numerical data. Similar flow structures at the streak breakdown are in fact observed for the unstable streaks in Brandt & Henningson (2002) and the transient growth scenario in Schoppa & Hussain (2002). Varicose modes are also shown to have significant amplifications and they are indeed observed in the simulations in Brandt *et al.* (2004). Comparable growth rates for varicose and sinuous modes are found in the analysis of the corrugated vortex sheet instability in Kawahara *et al.* (2003). Analysis of the equation governing the evolution of the perturbation kinetic energy reveals that the work of the Reynolds stress  $uw$  against the spanwise shear of the underlying streak is responsible for the transient growth of both sinuous and varicose disturbances. In both cases, the largest velocity component of the optimal disturbance is the spanwise whereas the optimal response is strongest in its streamwise velocity component. This also explains why the initial condition proposed by Schoppa & Hussain (2002) is able to trigger some transient amplification and lead to the streak breakdown. Future investigations will aim at a better understanding of the physical mechanism responsible for the observed transient growth and to quantify the realizability of this growth process in noisy situations in which streaks continuously form.

#### REFERENCES

- ANDERSSON, P., BERGGREN, M. & HENNINGSON, D. S. 1999 Optimal disturbances and bypass transition in boundary layers. *Phys. Fluids* **11**, 134–150.
- ANDERSSON, P., BRANDT, L., BOTTARO, A. & HENNINGSON, D. S. 2001 On the breakdown of boundary layers streaks. *J. Fluid Mech.* **428**, 29–60.
- BRANDT, L., COSSU, C., CHOMAZ, J.-M., HUERRE, P. & HENNINGSON, D. S. 2003 On the convectively unstable nature of optimal streaks in boundary layers. *J. Fluid Mech.* **485**, 221–242.

- BRANDT, L. & HENNINGSON, D. S. 2002 Transition of streamwise streaks in zero-pressure-gradient boundary layers. *J. Fluid Mech.* **472**, 229–262.
- BRANDT, L., SCHLATTER, P. & HENNINGSON, D. S. 2004 Transition in boundary layers subject to free-stream turbulence. *J. Fluid Mech.* **517**, 167–198.
- BUTLER, K. M. & FARRELL, B. F. 1992 Three-dimensional optimal perturbations in viscous shear flow. *Phys. Fluids A* **4**, 1637–1650.
- CORBETT, P. & BOTTARO, A. 2000 Optimal perturbations for boundary layers subject to stream-wise pressure gradient **12** (1), 120–130.
- COSSU, C. & BRANDT, L. 2004 On Tollmien-Schlichting-like waves in streaky boundary layers. *Eur. J. Mech./B Fluids* **23**, 815–833.
- FARRELL, B. F. 1988 Optimal excitation of perturbations in viscous shear flow. *Phys. Fluids* **31**, 2093–2102.
- FARRELL, B. F. & IOANNOU, P. J. 1993 Optimal excitation of three-dimensional perturbations in viscous constant shear flow. *Phys. Fluids A* **5**, 1390–1400.
- GROSSMANN, S. 2000 The onset of shear flow turbulence. *Reviews of Modern Physics* **72** (2), 603–618.
- KAWAHARA, G., JIMÉNEZ, J., UHLMANN, M. & PINELLI, A. 2003 Linear instability of a corrugated vortex sheet – a model for streak instability. *J. Fluid Mech.* **483**, 315–342.
- KIM, H. T., KLINE, S. J. & REYNOLDS, W. C. 1971 The production of turbulence near a smooth wall in a turbulent boundary layer. *J. Fluid Mech.* **50**, 133–160.
- LANDAHL, M. T. 1975 Wave breakdown and turbulence. *SIAM J. Appl. Maths* **28**, 735–756.
- LUCHINI, P. 2000 Reynolds-number independent instability of the boundary layer over a flat surface. Part 2: Optimal perturbations. *J. Fluid Mech.* **404**, 289–309.
- LUNDELL, F. 2004 Streak oscillations of finite length: Disturbance evolution and growth. *Phys. of Fluids* **16** (8), 3227–3230.
- MATSUBARA, M. & ALFREDSSON, P. H. 2001 Disturbance growth in boundary layers subjected to free stream turbulence. *J. Fluid. Mech.* **430**, 149–168.
- NAYFEH, A. H. & MOOK, D. T. 1979 *Nonlinear oscillations*. Wiley-Interscience.
- ORR, W. M. F. 1907 The stability or instability of the steady motions of a perfect liquid and of a viscous liquid. Part I: A perfect liquid. Part II: A viscous liquid. *Proc. R. Irish Acad. A* **27**, 9–138.
- SCHMID, P. J. & HENNINGSON, D. S. 2001 *Stability and Transition in Shear Flows*. New York: Springer.
- SCHOPPA, W. & HUSSAIN, F. 2002 Coherent structure generation in near-wall turbulence. *J. Fluid Mech.* **453**, 57–108.
- SWEARINGEN, J. D. & BLACKWELDER, R. F. 1987 The growth and breakdown of streamwise vortices in the presence of a wall. *J. Fluid Mech.* **182**, 255–290.
- WALEFFE, F. 1995 Hydrodynamic stability and turbulence: Beyond transients to a self-sustaining process. *Stud. Appl. Math.* **95**, 319–343.
- WEIDEMAN, J. A. C. & REDDY, S. C. 2000 A MATLAB differentiation matrix suite. *ACM Transaction of Mathematical Software* **26** (4), 465–519.